High-pressure structural and electronic properties of CuMO_2 (M = Cr, Mn) delafossite-type oxides

D. Levy,[1] E. Greenberg,[1] S. Layek,[1] M. P. Pasternak,[1] I. Kantor,[2,3] S. Pascarelli,[2,4] C. Marini,[2,5] Z. Konopkova,[6] and G. Kh. Rozenberg[1,*]

[1]*School of Physics & Astronomy, Tel-Aviv University, Ramat-Aviv, 69978, Tel Aviv, Israel*
[2]*European Synchrotron Radiation Facility, BP 220, 38043 Grenoble, France*
[3]*Technical University of Denmark, Fysikvej 311, 2800 Kgs. Lyngby, Denmark*
[4]*European XFEL, Holzkoppel 4, 22869 Schenefeld, Germany*
[5]*ALBA Synchrotron, Carrer de la Llum 2-26, 08290 Cerdanyola del Vallès, Barcelona, Spain*
[6]*DESY, Notkestr. 85, 22607 Hamburg, Germany*

(Received 14 December 2019; revised manuscript received 28 April 2020; accepted 14 May 2020; published 4 June 2020)

We report high-pressure x-ray diffraction, x-ray absorption spectroscopy, and electrical transport measurements on CuMO_2 (M = Cr, Mn) delafossitelike oxides in an attempt to study their structural and electronic evolution with pressure. Recent studies of the similar $CuFeO_2$ delafossite has revealed a pressure-induced breaking of the unusual high axial anisotropy resulting in a structural phase transition coinciding with the metal-metal intervalence charge-transfer phenomenon. The present study revealed other possible scenarios responsible for the collapse of the high axial anisotropy and evolution of the O-Cu-O bonds in delafossitelike materials under pressure. Thus in $CuMnO_2$, the O-Cu-O dumbbells tilt with respect to the c axis at $P > 13$ GPa, but in contrast to $CuFeO_2$, the tilting is continuous with pressure increase, justifying a second-order phase transition within the $C2/m$ structure. Meanwhile in $CuCrO_2$ ($R\bar{3}m$) the first-order structural phase transition to the monoclinic structure ($P2_1/m$) is observed at about 26 GPa characterized by the discontinuous bending of the O-Cu-O bond in contrast to the tilting in the case of $CuFeO_2$ and $CuMnO_2$. In both studied systems, we did not find clear evidence of valence transformations, similar to that observed in $CuFeO_2$.

DOI: 10.1103/PhysRevB.101.245121

I. INTRODUCTION

Cuprous delafossites ($Cu^+M^{3+}O_2$) exhibit exceptional electrical, magnetic, optical, and catalytic properties and are utilized for diverse technological applications as optoelectronic devices, field electron emitters, light-emitting diodes, laser diodes, solar cells, functional windows, and thermoelectric materials (Refs. [1,2] and references therein). The exceptional properties of these solids originate from the close interaction of the different metal cations in the mixed phase, which enables effects, not manifested in single-metal oxides [3]. One such effect recently discovered is a pressure-induced *metal-metal intervalence charge transfer* in $CuFeO_2$ [4].

The structure of all these cuprates at ambient conditions contains sheets of distorted, edge-sharing $M^{3+}-O$ octahedra linked by O-Cu^{1+}-O dumbbells, with the latter oriented along the c axis [Figs. 1(a) and 1(c)] [2]. Such a structure is characterized by a high axial anisotropy [$d(c/a)/dP > 0$] [5] arising from a weak axial compressibility of the O-Cu-O dumbbells. Such anisotropy is evidently unstable: as a result, in $CuFeO_2$ [space group (SG) = $R\bar{3}m$] [4] at $P\sim18$ GPa a transition to a more isotropic $C2/c$ structure with the O-Cu-O dumbbells tilting by 28° with respect to the c axis takes place. This transition is accompanied by a large drop in the molar volume V and in c/a, along with a sign reversal of its pressure derivative, $d(c/a)/dP < 0$, signaling the collapse of the high axial anisotropy. The long-range antiferromagnetic order stabilizes and, starting at ~23 GPa, the onset of Fe^{2+} species concurrent with a $Cu^{1+} \rightarrow Cu^{2+}$ partial transition; namely, a pressure-induced metal-metal charge transfer is observed. As a result the Cu^{2+}-O becomes fourfold coordinated and a new crystallographic structure with SG = $P\bar{3}m$ emerges. Similar high axial anisotropy and phase transitions between 18 and 34 GPa were reported also for $CuAlO_2$ [6] and $CuGaO_2$ [7] but only for $CuFeO_2$ were the structure of the high-pressure (HP) polymorphs identified.

In the present work, we report the results of high-pressure studies in two other delafossitelike systems, in which Mn^{3+} and Cr^{3+} substitutes for Fe^{3+}. These materials, $CuMnO_2$ (Crednerite) and $CuCrO_2$ (Mcconnellite), have peculiar magnetic properties that are widely studied at ambient pressure [8,9]. They both, similar to $CuFeO_2$, are a rather close approximation to a two-dimensional (2D) triangular-lattice antiferromagnet and, therefore, are an interesting family to study the effect of pressure on magnetism of low-dimensional systems. These compounds have similar layered features, but since the electronic configurations of Cr^{3+} and Mn^{3+} are different, there are some significant differences in the corresponding structures. While Cr^{3+} cations form a regular CrO_6 octahedron [10], the MnO_6 octahedron is strongly distorted due to the Jahn-Teller effect [11]. Correspondingly, in $CuMnO_2$ different directions in the triangular ab plane become inequivalent: this leads to a change of the crystal

*emtsm@tauex.tau.ac.il

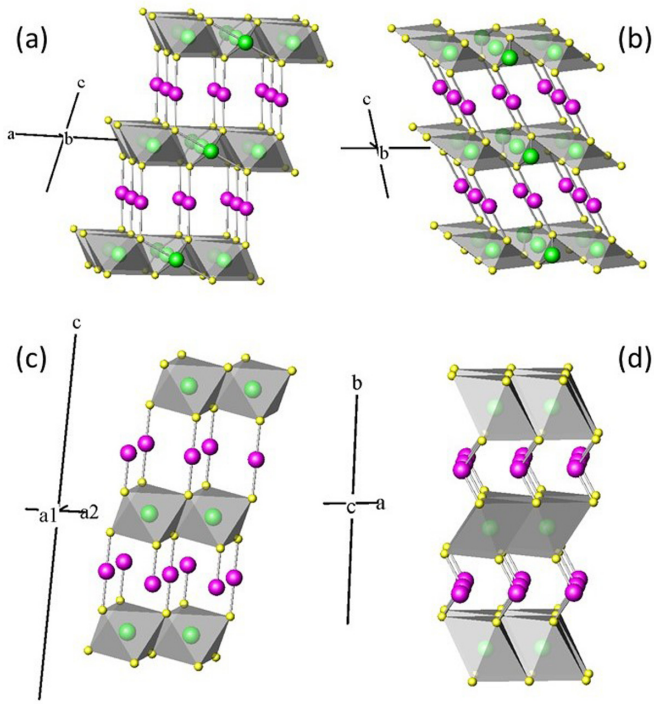

FIG. 1. The crystal structure ($C2/m$) of $CuMnO_2$ at 3 GPa (a) and at 40 GPa (b). The crystal structures of $CuCrO_2$: $R\bar{3}m$ at 3 GPa (c) and $P2_1/m$ at 31 GPa (d) (HP1 phase). The large magenta (shiny) and small yellow (shiny) spheres correspond to the Cu^{1+} and O^{2-} ions, large -green spheres to the Mn^{3+}/Cr^{3+}, respectively.

structure from the usual delafossite rhombohedral to a monoclinic structure already at ambient conditions. Namely, the stacking orientation of M^{3+}-O layers and O-Cu^{1+}-O dumbbells results in two different polymorphs: a rhombohedral (SG $R\bar{3}m$) in $CuCrO_2$, similar to $CuFeO_2$, and in $CuMnO_2$, due to a mismatch between the slices, a distorted monoclinic ($C2/m$) (Fig. 1).

At ambient pressure, $CuMnO_2$ undergoes a phase transition at $T_N = 65$ K to a strained triclinic $C\bar{1}$ structure which is claimed to be responsible for the frustration collapse (2D → 3D) (three-dimensional) [12]. In general, the reason for the low-dimensionality, 2D, which leads to spin frustration is the relative weak interlayer superexchange $J_{M_1-M_2}$ interaction as compared with intralayer $J_{M_1-M_1}$ within the a-b plane. Pressure can add a new *dimension* in elucidating the mechanism of dimensionality crossover, and indeed, HP–XRD (x-ray-diffraction) studies in $CuFeO_2$ have shown that the 2D state collapses with pressure at about 18 GPa [13], which coincides with the transition into a more isotropic $C2/c$ structure and the change in slope of $c/a(P)$ from positive to negative [4]. Undoubtedly, study of other delafossitelike systems, with different symmetry, may provide valuable experimental basis for a better understanding of the structural and electronic properties of such materials. The present study was performed up to about 58 GPa combining methods of synchrotron XRD and x-ray absorption spectroscopy (XAS) at the Cr, Mn, and Cu K edges, allowing us to follow the possible pressure-induced structural transitions and to test the possibility of concurrent electronic transformations similar to $CuFeO_2$. This study has revealed other possible scenarios responsible for the collapse of the high axial anisotropy upon compression, and their consequences upon the electronic properties of the $CuMO_2$ (M = Cr, Mn) cuprates.

II. EXPERIMENT

Samples of $CuCrO_2$ and $CuMnO_2$ were prepared by solid-state reaction of chromium/manganese and cupric oxides. High-purity (99.999%) powders of these oxides in stoichiometric ratio were thoroughly mixed, ground, pelletized, and heated to 800 °C for 12 h. The $CuCrO_2$ sample was prepared in an ambient atmosphere while the $CuMnO_2$ under vacuum in a quartz sealed ampule in order to prevent the oxidation of Mn^{3+}. After cooling to room temperature, the pellet was ground, mixed, pressed, heated, and cooled again under the same conditions. Its structure and purity were verified with x-ray powder diffraction by using a standard laboratory instrument. The sample was placed inside cylindrical cavities of a Re gasket following indentation to 30-μm thickness. TAU miniature piston-cylinder diamond-anvil cells (DAC) and PETRA membrane cells were used to generate pressures [14]. The anvil culets ranged from 250 to 300 μm in diameter with sample cavities from 120 × 30 μm to 150 × 50 μm. Ne was used as a pressure-transmitting medium for both XRD and XAS studies. Pressure was measured using the ruby $R1$ fluorescence line as a pressure marker using the calibration scales mentioned in Ref. [15].

XRD experiments have been performed at the Extreme Conditions Beamline P02.2 at PETRA III, Hamburg, Germany ($\lambda = 0.289\,53$ Å). XRD measurements were carried out at room temperature (RT) up to 50 GPa in angle-dispersive mode with patterns collected using a PerkinElmer flat-panel detector and integrated using the FIT2D program [16,17]. The resulting diffraction patterns were analyzed with the GSAS program [18,19].

XAS was performed at the energy-dispersive beamline ID24 of the European Synchrotron Radiation Facility, Grenoble, employing a Si(111) polychromator and three Si mirrors for harmonic rejection and vertical focusing [20]. The focal spot was $\sim 5 \times 5\,\mu m^2$ full width at half maximum, and use of partially perforated anvils [21] substantially reduced x-ray absorption by the diamonds at the Cu, Cr, and Mn K edges. Detector pixel to energy second-order polynomial conversion parameters were obtained by fitting reference Cu, Cr, and Mn foils spectra. We note that in the current experiment, we implemented a partially perforated (PP) diamond anvil with a special design (see Supplemental Material Fig. S1 [22]). Such a special design allows: (i) alignment of PP culets and the use of ruby fluorescence overcoming the issue of opaque to visible light walls of the perforated conical holes, and (ii) overcomes the fragility at high pressures of the previously used *miniature anvil* [20] without compromising the thin diamond windows into the 100-GPa range to collect the x-ray absorption signal at low energy. XAS measurements were carried out up to 23 GPa for Cu K edge and 35 GPa for Mn K edge for $CuMnO_2$, and up to about 50 GPa for Cu- and Cr K edge for $CuCrO_2$. The experimental x-ray absorption near-edge structure (XANES) spectra were reduced by subtracting a linear pre-edge background and normalizing the post-edge

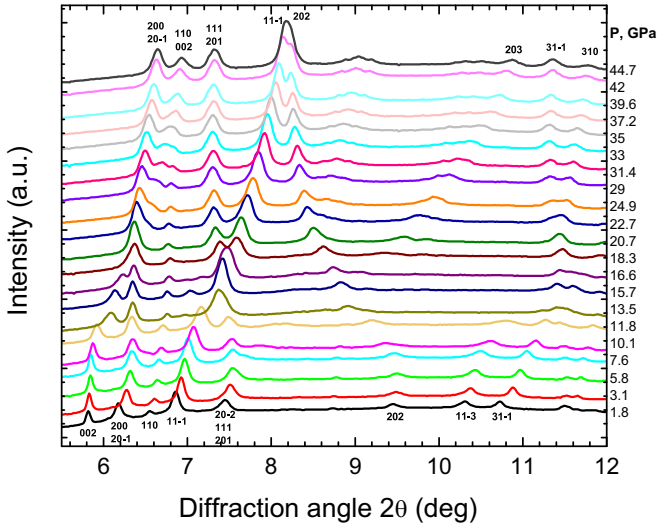

FIG. 2. X-ray powder-diffraction patterns of $CuMnO_2$ at RT at various pressures.

jump to unity. The energy of the edge position was taken as the first maximum of the absorption coefficient energy derivative.

Electrical transport measurements up to $P \sim 58$ GPa were performed using TAU piston-cylinder DACs. Pressed powder samples were loaded into 100-μm-diameter cavities drilled in a rhenium gasket insulated with a layer of Al_2O_3-NaCl (3:1 atomic ratio) mixed with epoxy, which also serves as the pressure medium. Six platinum triangles, serving as electrodes, were placed on the culet to permit measurements in various DC four-probe arrangements at a given pressure. The Pt electrodes were connected to exterior conducting wires by a silver epoxy. Resistance was measured as a function of pressure and temperature (for both compression and decompression cycles) using a standard four-probe method in a custom-made cryostat. At each temperature, the voltage was measured as a function of a series of applied currents, for determining the resistance from the obtained slope. The temperature was measured using a Lakeshore Si (DT-421-HR) diode in proximity to the DAC. Few ruby fragments were placed in the center region of the culet between the Pt electrodes overlapping the sample for pressure calibration. Pressure was measured both before and after each measurement from the ruby fluorescence spectra. Pressure gradients were measured to be small (~5%) in the distances 15–20 μm between the tips of the Pt electrodes across which voltage was measured.

III. RESULTS

A. X-ray diffraction

1. $CuMnO_2$

Diffraction patterns of $CuMnO_2$ collected at different pressures are shown in Fig. 2. As can be seen, in $CuMnO_2$ up to ~12 GPa all peaks except (0,0,2) move to higher 2θ values but the behavior of most peaks, e.g., (1,1,−1), (2,0,−2), and *(2,0,2)*, is nonlinear and, in some cases, nonmonotonous. The most drastic change we observe at ~13 GPa: the (0,0,2) peak shifts significantly to a higher 2θ value while peak (2,0,0) moves in the opposite direction. In the opposite direction (2,0,−2), (2,0,2), and some other peaks move promptly also

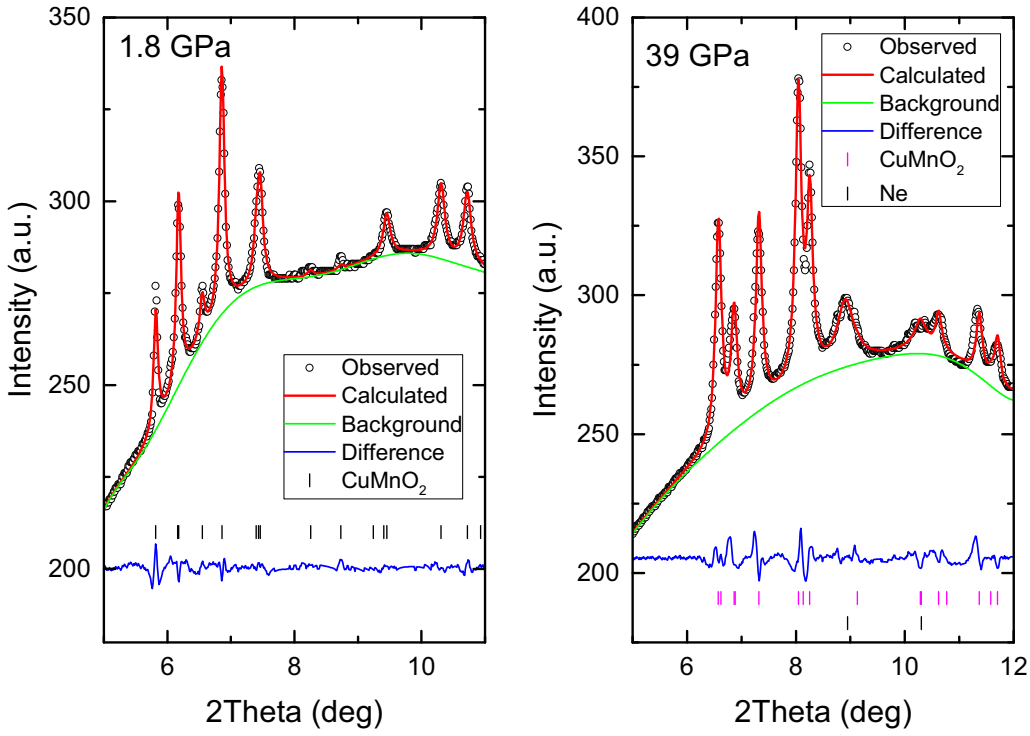

FIG. 3. Typical examples of analyzed integrated patterns of $CuMnO_2$ collected at 1.8 and 39 GPa, respectively, assuming a $C2/m$ structure. The refinements have been performed on 33 observables and 20 variables, χ^2 is about 1.8. In the diffractogram at 39 GPa the Ne peaks are the ones with black tick marks ($\lambda = 0.289\,53$ Å).

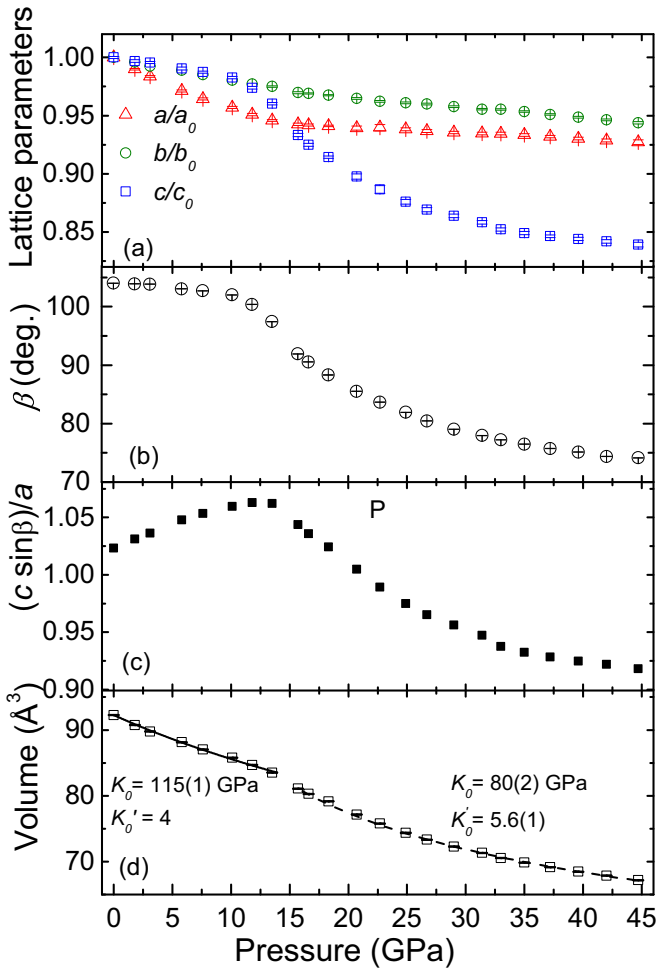

FIG. 4. Variations of normalized unit-cell parameters (a), the monoclinic angle β (b), crystal anisotropy (c), calculated as the c*sinβ/a ratio, and unit-cell volume (d) of $CuMnO_2$ as a function of pressure. The solid and dashed lines are fits for two pressure ranges, 0–13.5 GPa and 15.7–45 GPa, using BM EOS.

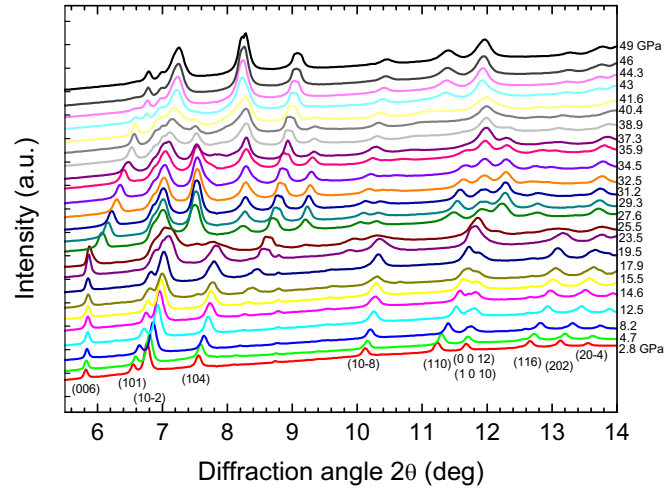

FIG. 5. X-ray powder-diffraction patterns of $CuCrO_2$ at RT at various pressures.

(Fig. 2). However, it is noteworthy that up to the highest pressure measured no new peaks appear and the experimental diffraction patterns could be satisfactorily fitted with the distorted monoclinic $C2/m$ structure [23] [see Figs. 3(a) and 3(b)] with the weighted residual and residual agreement factors wRp being less than 1.9% and Rp less than 1.2%, respectively. This structure can be completely characterized by the three lattice parameters *a, b, c*, and the monoclinic angle β, with the fixed Cu position (0, 1/2, 1/2), the Mn position (0, 0, 0), and the oxygen position (x, 0, z). The numerical results of the refinement are summarized in Table S1 (Supplemental Material [22]).

The unit-cell parameters, the monoclinic angle β, crystal anisotropy, calculated as the ratio between cell height (c*sinβ) and a parameter as a function of pressure are shown in Fig. 4. Up to ∼12 GPa, the b and c parameters, as well as the β angle, barely change with pressure and the main compression takes place along the a axis. However, above ∼12 GPa the compression features change drastically, the a axis ceases to shrink and its behavior starts to be similar to b axis compression; meanwhile, the c axis start to decrease promptly. Moreover, the monoclinic angle β strongly diminishes passing from obtuse to acute (from 102° at 10.1 GPa to 82° at 24.9 GPa and further to 74.1° at 44.7 GPa).

The volume versus the pressure dependence [Fig. 3(d)] also confirms significant structural alterations around 12 GPa: clear change of the compressibility is observed at this pressure range. Correspondingly, two different equations of state (EOS) should be used above and below 13.5 GPa. Splitting into two ranges, 0–13.5 GPa and 15.7–45 GPa, using Birch-Murnaghan (BM) EOS [24] results in $K_0 = 115(1)$ GPa, $K_0' = 4$ (fixed) and $V_0 = 92.27.(3)$ Å^3, and $K_0 = 80(2)$ GPa, $K_0' = 5.6(1)$, and $V_0 = 83.2(2)$ Å (Fig. 4), respectively, where K_0, K_0', and V_0 are the bulk modulus, its pressure derivative, and the unit-cell volume at 1 bar and 300 K, correspondingly. It is noteworthy that the observed structural changes are reversible with no noticeable hysteresis in pressure, which confirms an isostructural feature of the observed structural transformations.

2. $CuCrO_2$

Diffraction patterns of $CuCrO_2$ collected at different pressures are shown in Fig. 5. As can be seen, in $CuCrO_2$ no appreciable changes in XRD spectra have been observed up to ∼20 GPa and the experimental diffraction patterns could be satisfactorily fitted with the rhombohedral $R\bar{3}m$ structure [25] [see Fig. 6(a)]. This low-pressure (LP) structure can be completely characterized by the two lattice parameters a and c, the Cu position (0,0,0), the Cr position (0, 0, 1/2), and the oxygen position (0, 0, z). Those parameters have been refined with wRp being less than 1.7% and Rp less than 1.1%. The numerical results of the refinement are summarized in Table S2 (Supplemental Material [22]).

At $P \sim 18$ GPa some broadening of the peaks of the LP phase is observed and around 23.5 GPa an array of additional peaks appears (Fig. 5). This structure, designated as the HP1 phase, coexists with the LP phase and its relative abundance increases with rising pressure, reaching 100% at ∼29 GPa. The diffraction patterns of the HP1 phase have been

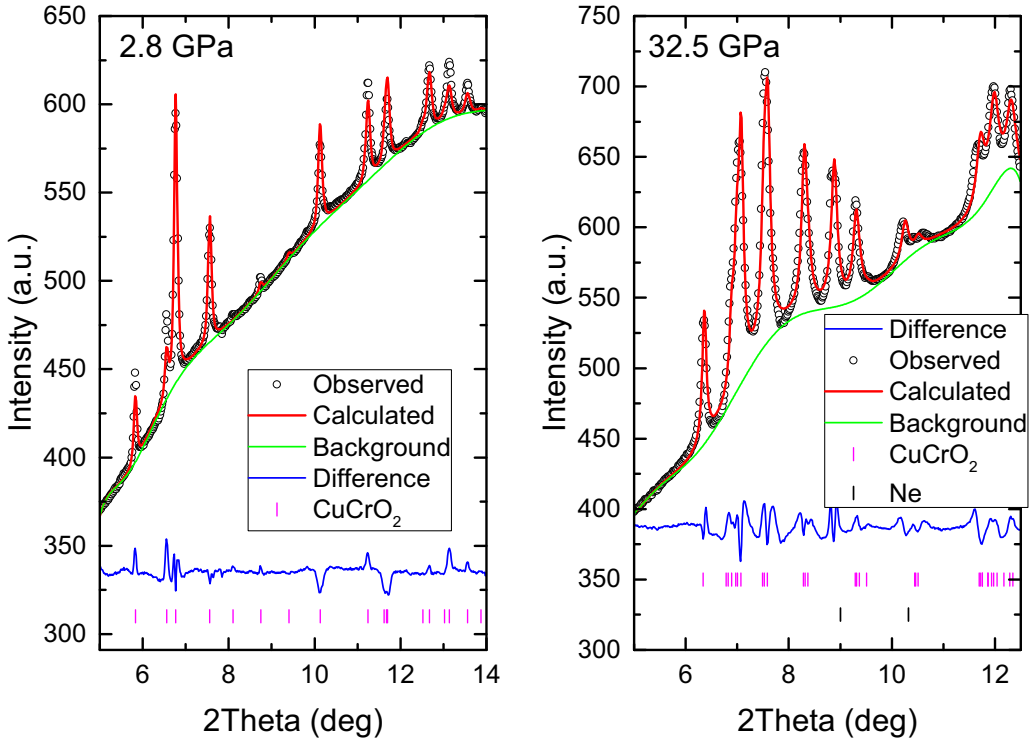

FIG. 6. Typical examples of analyzed integrated patterns of $CuCrO_2$ collected at 2.8 and 32.5 GPa, respectively, assuming $R\bar{3}m$ symmetry for low-pressure phase and a $P2_1/m$ for the high-pressure phase ($\lambda = 0.289\,53$ Å). The refinements for the hexagonal phase have been performed on 50 observables and 24 variables, χ^2 is about 3; for the monoclinic phase, on 50 observables and 20 variables, χ^2 is about 2.4.

satisfactorily fitted with a monoclinic model with $P2_1/m$ symmetry [Fig. 6(b)] with $wRp < 2.1\%$ and $Rp < 1.4\%$. We note that the observed onset of the first-order structural phase transition around 23.5 GPa is in good agreement with results of Raman spectroscopy studies suggesting a structural phase transition around 24.5 GPa [2,26].

The numerical results of the refinement are summarized in Table S2 (See Supplemental Material [22]). Similar to $R\bar{3}m$ it is also a layered structure obtained by layers displaced in the *ab* plane, resulting in a bending of the rigid O-Cu-O "dumbbells" (Fig. 1). The unit-cell parameters, volume, and crystal anisotropy, calculated as the ratio between *c* and *a* parameters, as a function of pressure are shown in Fig. 7. The $V(P)$ data for the LP and HP1 phases can be fitted well with a second-order Birch-Murnaghan EOS ($K_0' = 4$, fixed) which yields the following values: $K_0 = 164(8)$ GPa, $V_0 = 131.0(5)$ Å^3 and $K_0 = 135(17)$ GPa, $V_0 = 87(1)$ Å^3 for the LP and HP1 phases, respectively. We note that the K_0 value obtained for the LP phase is in good agreement with the value reported recently by Garg *et al.* [$K_0 = 156.7(2.8)$ GPa, $K_0' = 5.3$] [26]. The obtained interatomic distances and O-Cu-O bond angle are shown in Fig. 8.

At *P* 43 GPa a group of additional peaks appears and above 44 GPa the peaks corresponding to the $P2_1/m$ structure disappear (Fig. 5). The unambiguous determination of a structure of this phase, designated as the HP2 phase, is complicated because of strong broadening of the peaks. However, it seems that the HP2 phase has a higher symmetry compared to the HP1 phase due to the significant decrease in the observed number of peaks.

Upon decompression from 50 GPa $CuCrO_2$ goes back to the low-pressure phase LP passing through the intermediate high-pressure phase HP1 as can be seen in Fig. S2 (Supplemental Material [22]). These structural transformations show pressure intervals not very different from the ones observed during compression.

B. X-ray absorption spectroscopy

1. $CuMnO_2$

Cu and Mn *K*-edge x-ray absorption near-edge structure spectra of $CuMnO_2$ at various pressures are shown in Fig. 9. One can see that the features of the Mn spectra barely change with pressure, while some important alterations are visible in the XANES spectra of Cu. Namely, at about 13 GPa a peak (B) at ~8984 eV appears and its intensity increases with pressure while two LP peaks around 8978 (A) and 8995 eV (D), respectively, strongly weaken. The variation of the position of the Cu and Mn *K*-edge absorption onset with pressure rise is shown in Figs. 10(a) and 10(b). One can see that the Cu *K*-edge absorption onset energy increases sharply by ~0.9 eV between 14 and 19 GPa, whereas the Mn *K*-edge absorption onset does not show a significant change at this pressure range.

2. $CuCrO_2$

The behavior of Cu *K*-edge XANES spectra of $CuCrO_2$ with pressure increase is very similar to $CuMnO_2$ case (Fig. 11). Namely, above 22 GPa, with the transition to the

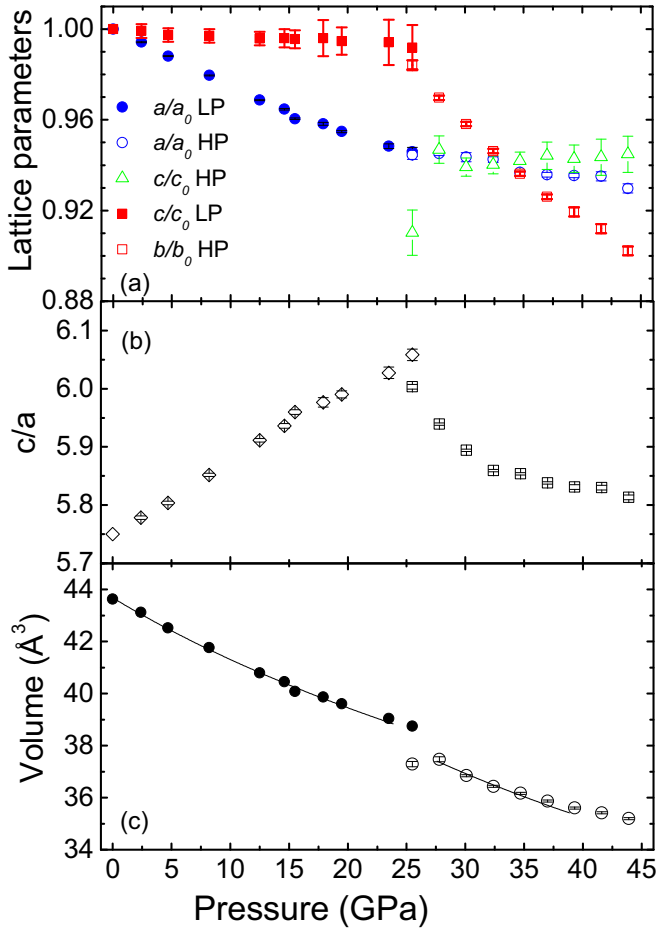

FIG. 7. Variations of the normalized lattice parameters (a), unit-cell volume (c), and crystal anisotropy (b), calculated as the c/a ratio of $CuCrO_2$ as a function of pressure. The solid and dashed lines are theoretical fits for the $R\bar{3}m$ and $P2_1/m$ phases using BM2 EOS. The volume was normalized to three unit formulas of $CuCrO_2$, i.e., $Z = 3$ for $R\bar{3}m$ phase and $Z = 2$ for $P2_1/m$ phase.

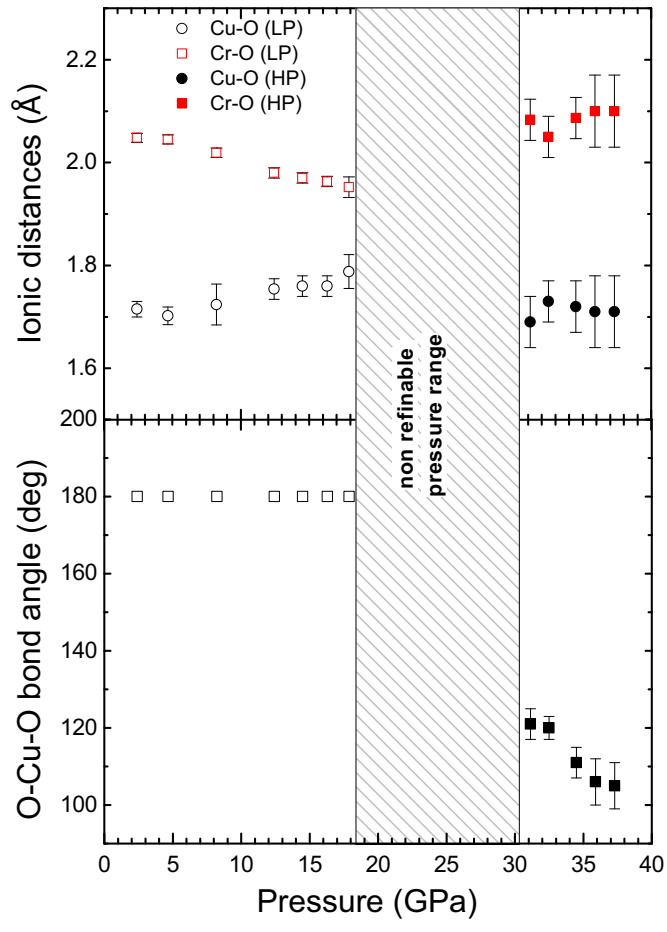

FIG. 8. Variation of the mean Cr-O, Cu-O distances and O-Cu-O bond angle in $CuCrO_2$ as a function of pressure.

HP1 phase, a peak appears at ~8984 eV (B) and its intensity increases with pressure while two LP peaks around 8978 (A) and 8995 eV (D), respectively, weaken. These changes corroborate with appreciable alterations of the XANES spectra at the Cr K edge: a peak at ~6001 eV appears while the peak at 6006.7 eV moves to 6008.3 eV and another one at ~6015 eV disappears. Above 40 GPa a substantial change has been observed in the features of the XANES spectra of $CuCrO_2$ at the Cr and Cu K edges: namely, significant change in the positions of the main peaks. In contrast to $CuMnO_2$ the Cu and Cr K-edge absorption onset do not show any special features at the pressure range of the transitions from LP to HP1, and from HP1 to HP2 phases: the Cu and Cr K-edge absorption onset energy sluggishly increases or decreases, respectively, from 10 to ~50 GPa [Figs. 10(c) and 10(d)] [27].

C. Electrical transport measurements

Resistance R as function of pressure up to about 58 GPa measured for $CuCrO_2$ at $T = 300$ K is plotted in Fig. 12(a). R hardly changes with increasing pressure up to about 20 GPa

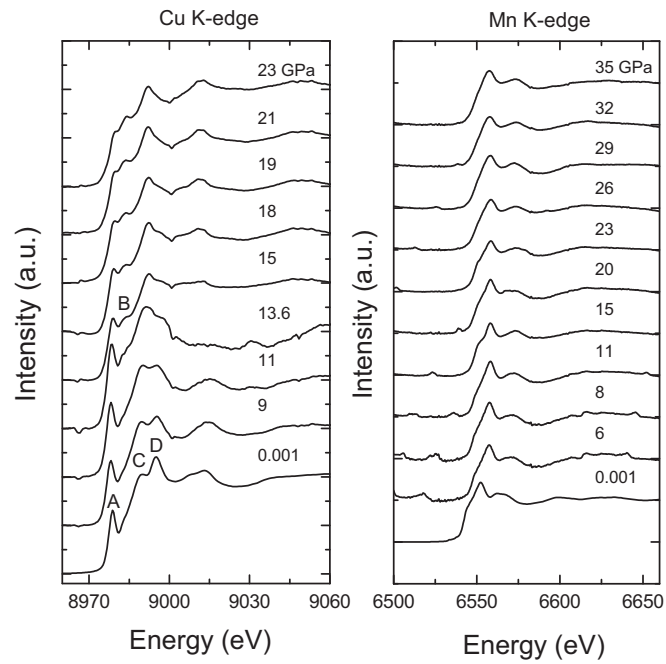

FIG. 9. Cu and Mn K-edge XANES spectra of $CuMnO_2$ at various pressures.

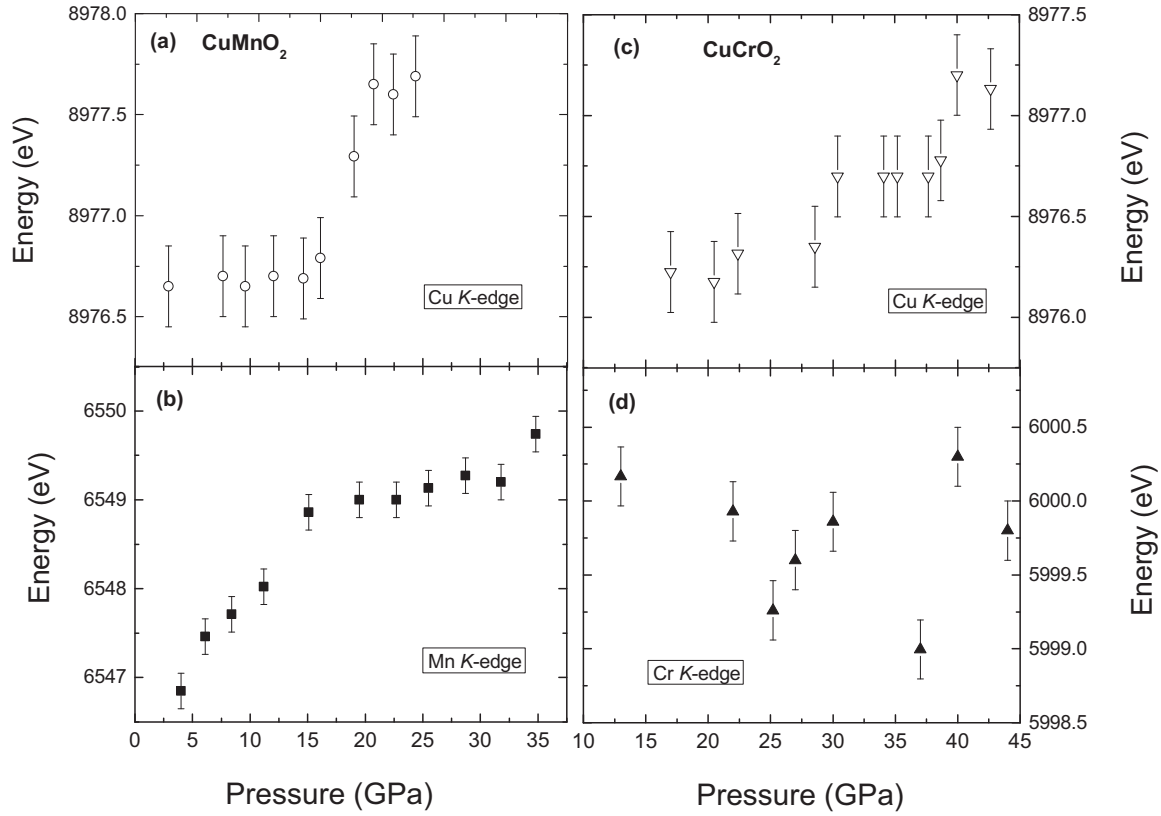

FIG. 10. The energy of the Cu and Mn *K*-edge absorption onset in $CuMnO_2$ (a), (b), and the energy of the Cu and Cr *K*-edge absorption onset in $CuCrO_2$ (c), (d) as a function of pressure.

after which a steep decrease by more than two orders of magnitude is found, followed by a change of the slope of $R(P)$ curve around 30 GPa. A steeper decrease in R is observed again above 45 GPa with gradual flattening above 52 GPa.

Figure 12(b) shows the temperature dependent $R(T)$ at various pressures. All $R(T)$ data display, within the studied temperature range, a temperature dependence consistent with insulating behavior up to the highest pressures measured. These data rule out any metallic state at pressures up to 58 GPa for $CuCrO_2$. The resistance variations with temperature at various pressures were first plotted in terms of Arrhenius and small polaron models, as $\ln R^{-1}$ vs T^{-1} and then as $\ln R^{-1}T$ vs T^{-1}. However, no significant straight-line region was observed in these graphs. We show in Fig. 12(c) plots of $\ln R$ vs $(T_0/T)^{1/4}$, these being indicative of three-dimensional variable range-hopping law [28,29] where T_0 is the Mott temperature. At 20 GPa this mechanism is applicable over the whole measured temperature range, down to 180 K, while at pressures 30.5 GPa and above at a temperature of ∼200 K a change of the slope is observed. This points to prevailing complex conductivity mechanisms likely involving both Cu and Cr species. Estimates of the Mott temperature and its pressure evolution are obtained from the slopes of linear regions of such plots [see Fig. 12(a), inset]. T_0 changes by more than one order of magnitude in going from the $CuCrO_2$-LP to the HP1 phase, and then decreases gradually with pressure without an appreciable change at the HP1–HP2 structural transition.

IV. DISCUSSION

As was mentioned above, the characteristic feature of the $M^{3+}Cu^{+1}O_2$ cuprates, which represent a rather close approximation to a 2D triangular-lattice antiferromagnet, is a large axial anisotropy with $d(c/a)/dP > 0$ [4,5]. Such axial anisotropy results from the presence of rigid (O-Cu^{1+}-O) dumbbells (Fig. 1) oriented along the c axis. Such anisotropy is evidently unstable at high pressure, as was shown earlier in the case of $CuFeO_2$ delafossite [4], where a transition to a more isotropic $C2/c$ structure with the O-Cu-O dumbbells tilting by 28° with respect to the c axis was found. This axial anisotropy was evidently observed at low pressures also in the studied $CuMnO_2$ and $CuCrO_2$ systems, culminating with a total increase of the crystal anisotropy parameter, $c\sin\beta/a$ and c/a, respectively, ∼4 and 5% with respect to ambient pressure at 13 and 25.5 GPa in $CuMnO_2$ and $CuCrO_2$, respectively (Figs. 4 and 7). Moreover, similar to $CuFeO_2$, this anisotropy does not survive under pressure: $CuMnO_2$ and $CuCrO_2$ also undergo a structural transformation upon compression. However, in the case of $CuMnO_2$ and $CuCrO_2$ other scenarios of the collapse of the high axial anisotropy are realized.

Thus, similar to the $CuFeO_2$ delafossite, the LP $R\bar{3}m$ phase of $CuCrO_2$ is characterized by an unusual pressure-induced anisotropy with a significant increase in c/a ratio with increasing pressure because main compression takes place along the a axis. Moreover, similar to the Fe-delafossite the first order structural transition above ∼20 GPa results in a reversal of the c/a slope and prompt decrease of the c parameter while

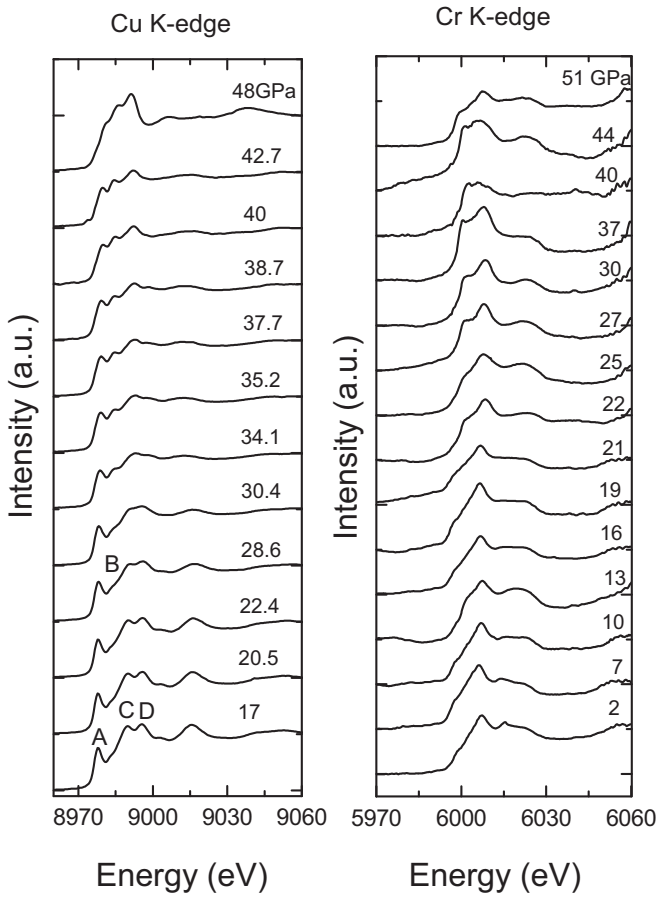

FIG. 11. Cu and Cr *K*-edge XANES spectra of $CuCrO_2$ at various pressures.

the *a*- and *b* axis barely change with pressure. However, in the present case instead of the tilting of the rigid dumbbells, maintaining the O-Cu-O angle of 180°, we observe a bending of this bond during the structural transition.

The pressure dependencies of the interatomic distances and O-Cu-O bond angle are shown in Fig. 8 (see also Supplemental Material Fig. S3 [22]). In these graphs, the pressure range between 18 and 29 GPa is excluded because at the coexistence range the refinement of the oxygen positions is not reliable. One can see that with the transition to the HP1 phase the Cr-O polyhedron expands and the Cu-O, Cu-Cu, Cu-Cr distances shrink. These alterations corroborate with a discontinuous reduction of the O-Cu-O bond angle (from 180° to ∼120° at 29 GPa), which continues to decrease with further pressure raise to ∼105° at 37 GPa. The transition to the HP1 phase is accompanied also by an appreciable reduction of the crystal volume (∼3%).

Meantime, in the case of $CuMnO_2$, in contrast to Fe- and Cr delafossites, no symmetry change was observed up to ∼45 GPa. The XRD studies have shown that, similar to $CuFeO_2$, the O-Cu-O dumbbells in $CuMnO_2$ start tilting with respect to the *c* axis at $P > 13$ GPa [Fig. 5(b)] but the tilting is continuous with pressure increase. Furthermore, there is no abrupt change of lattice parameters (Fig. 5). However, a rather prompt decrease of the *c* parameter and the monoclinic angle β starts above 11.8, resulting in a strong change of the crystal anisotropy: namely, in a sign reversal of $c\sin\beta/a$ pressure derivative from positive to negative. Thus, if the compressions of the unit cell are firstly driven by the *a*-axis shrinkage, above ∼13 GPa the *c* axis and the β angle change define the unit-cell behavior. We note that the change of the latter two is governed by the change of the angle α between the sheets of M^{3+}-O octahedra and linear (O-Cu^{1+}-O) dumbbells (see Fig. 13). The α angle barely changes up to 13 GPa but starts to decrease rapidly above this pressure due to the continuous dumbbells tilting, reaching ∼53° at 44 GPa. The continuous nature of all of the above-mentioned changes allows us to suggest that a second-order phase transition takes place in the present case.

It is noteworthy that in both systems destruction of the low-pressure structural construction, characterized by the rigid O-Cu-O dumbbells situated perpendicular to the MO_6 slabs, results in a softening of the materials and a significant decrease of bulk modulus values, namely, from 115 to 80 GPa at the transition pressure of 14 GPa and from 164 to 135 GPa at the transition pressure of 25 GPa, for $CuMnO_2$ and $CuCrO_2$, respectively.

Another important feature recently discovered in $CuFeO_2$ delafossite [3] is the pressure-induced metal-metal *intervalence charge transfer* following the collapse of the high axial anisotropy. Starting at ∼23 GPa, the onset of Fe^{2+} species concurrent with a $Cu^{1+} \rightarrow Cu^{2+}$ partial transition triggered by the increase in overlap of atomic orbitals is observed followed by the structural transition and Cu coordination number increase. The question is if a similar phenomenon could be observed in Cr- and Mn delafossites. We note that usually in XAS studies orbital reorganization would change spectral features, while valence change would result in the edge shift. For example, in $CuFeO_2$ the authors observed the sharp edge shift on the order of 1 eV in opposite directions for Cu and Fe ions in the 20–30-GPa range, consistent with a valence transformation $Cu^{1+} \rightarrow Cu^{2+}$ and $Fe^{3+} \rightarrow Fe^{2+}$ proposed from the Mössbauer data analysis. With this, one should take into account that the edge position may change also if there are changes of local environment, metal-ligand distances, etc. Thus, in Fe oxides edge shift of about +1 eV is observed by a simple compression from 0 to ∼50 GPa. This means that if we look at the edge position as a function of pressure, a continuous variation does not prove any valence change, while a "jump" is more convincing. In the case of $CuCrO_2$ no jumps have been observed at the studied pressure range and correspondingly no evidence for Cu or Cr oxidation state changes. Meanwhile, for $CuMnO_2$ there is a steep change of about 0.9 eV of the Cu *K*-edge position between 14 and 19 GPa suggesting that copper increases in oxidation state. However, the absence of a corroborating negative shift of the Mn *K* edge at this pressure range casts doubt on the idea of the pressure-induced metal-metal intervalence charge transfer in the present case. Taking into account the behavior of the Mn *K* edge and significant structural changes observed at this pressure range (strong tilting of the O-Cu-O dumbbells with respect to the sheets of M^{3+}-O octahedra), we suggest that the change of the Cu *K*-edge position could be related to the above-mentioned structural alterations which affect local environment and metal-ligand distances [30].

It is noteworthy that similar to $CuFeO_2$, despite two pressure-induced structural phase transitions, $CuCrO_2$

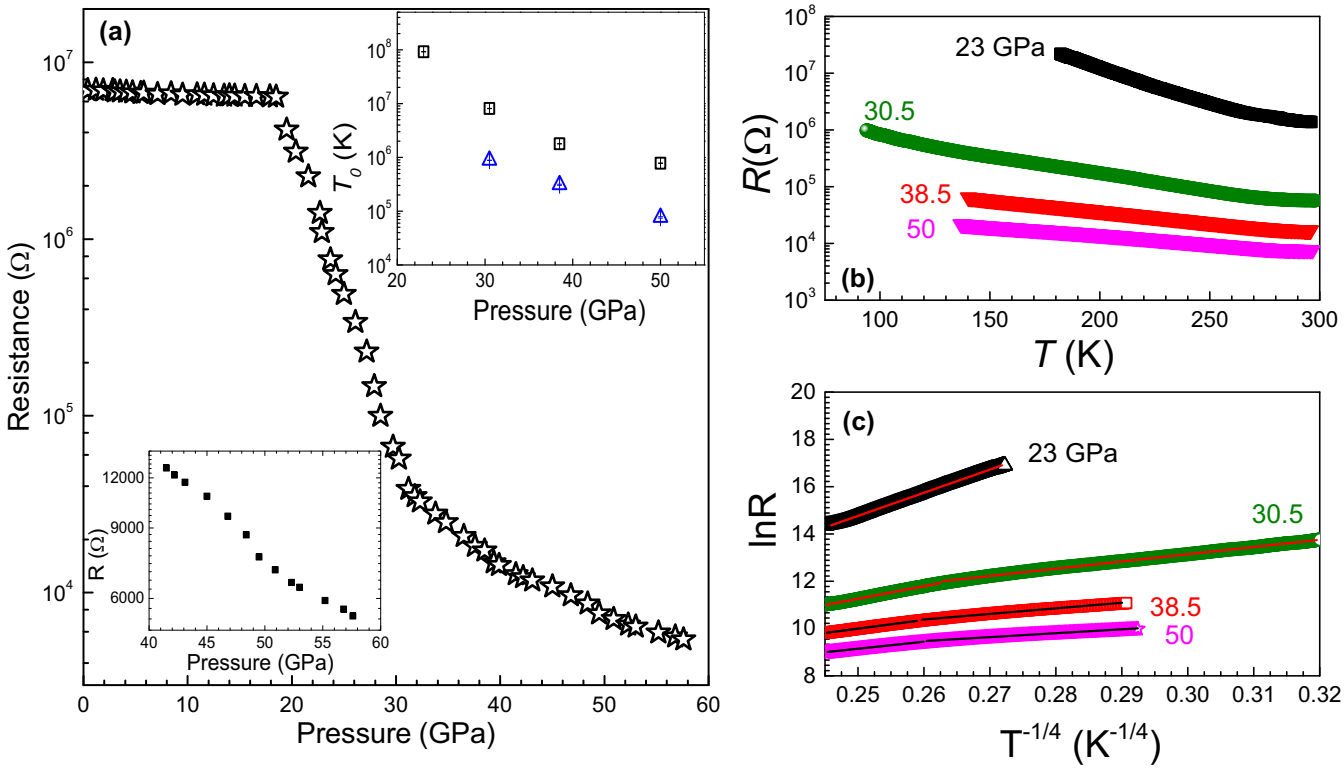

FIG. 12. (a) Pressure dependence of the resistance at 300 K for $CuCrO_2$. (b) Temperature dependence of the resistance measured at various pressures. (c) Linearized temperature-dependent data at various pressures assuming variable range-hopping mechanism, $\ln R \propto (T_0/T)^{1/4}$. The Mott temperature T_0 is obtained from the slope of linear fits to these plots for two temperature ranges, above and below ~200 K. Inset [panel (a)] shows the pressure dependence of T_0 for two temperature ranges: above and below ~200 K (squares and triangles, respectively).

remains nonmetallic as manifested in persistent semiconducting behavior and a relatively large Mott temperature value in the range of 50 GPa, about 10^5-10^6 K; see Fig. 12(a). The first structural transition around 25 GPa results in the decrease of T_0 by about one order of magnitude but following that only a rather slight T_0 decrease is observed. This estimates a hint at charge-carrier localization being persistent up to about 100 GPa, if there is no drastic structural transition to radically change the electronic band structure.

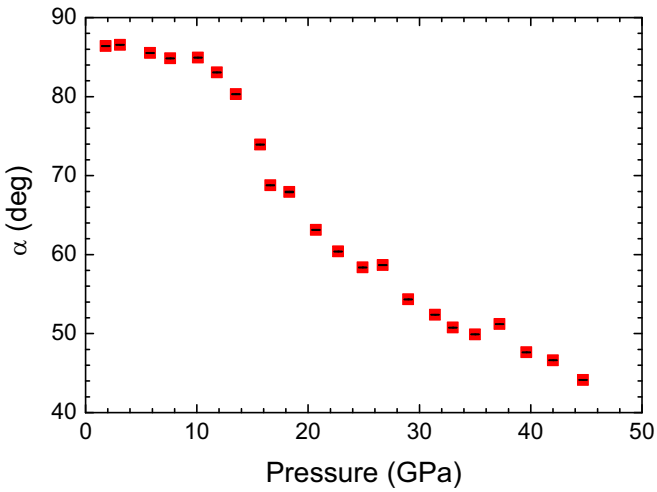

FIG. 13. Pressure dependence of the α-angle between the sheets of M^{3+}-O octahedrons and linear (O-Cu^{1+}-O) dumbbells for $CuMnO_2$.

In summary, our studies of $CuMO_2$ (M = Cr, Mn) cuprates reveal different scenarios of the breaking of the high axial anisotropy and evolution of the O-Cu-O bonds in delafossitelike materials under pressure. In $CuCrO_2$ the first-order structural phase transition to the monoclinic structure ($P2_1/m$) is observed at about 26 GPa, triggered by the structural instability of $R\bar{3}m$ under pressure, and characterized by the discontinuous bending of the O-Cu-O bond in contrast to the tilting in $CuFeO_2$. Meanwhile in $CuMnO_2$, characterized at ambient pressure by the monoclinic structure ($C2/m$) due to the Jahn-Teller distortion of Mn^{3+}, the O-Cu-O dumbbells start tilting with respect to the c axis at $P > 13$ GPa, but in contrast to $CuFeO_2$, the tilting is continuous with pressure increase, justifying a second-order phase transition within the $C2/m$ structure. Cu, Cr, and Mn K-edge XANES and extended x-ray-absorption fine-structure studies, carried out to clarify the issue of valence transformations, similar to that observed in $CuFeO_2$, did not find clear evidence of such phenomenon in the studied systems. With that, similarly to $CuFeO_2$, $CuCrO_2$ demonstrates the persistent semiconducting behavior up to the highest pressures measured. We believe that the present study adds insight into the complexity of transition-metal oxides in the regime of high density of matter.

ACKNOWLEDGMENTS

This research was supported by the Israel Science Foundation (Grants No. 1189/14 and No. 1552/18). S.L. thankfully acknowledges Planning and Budgeting Committee (PBC) of the Council for Higher Education in Israel for postdoctoral fellowship.

[1] A. P. Amrute, Z. Lodziana, C. Mondelli, F. Krumeich, and J. Perez-Ramirez, Chem. Mater. **25**, 4423 (2013).

[2] A. B. Garg and R. Rao, Crystals **8**, 255 (2018).

[3] F. X. Redl, K.-S. Cho, C. B. Murray, and S. O'Brien, Nature (London) **423**, 968 (2003).

[4] W. M. Xu, G. K. Rozenberg, M. P. Pasternak, M. Kertzer, A. Kurnosov, L. S. Dubrovinsky, S. Pascarelli, M. Munoz, M. Vaccari, M. Hanfland, and R. Jeanloz, Phys. Rev. B **81**, 104110 (2010).

[5] T. R. Zhao, M. Hasegawa, T. Kondo, T. Yagi, and H. Takei, Mater. Res. Bull. **32**, 151 (1997).

[6] J. Pellicer-Porres, A. Segura, C. Ferrer-Roca, A. Polian, P. Munsch, and D. Kim, J. Phys.: Condens. Matter **25**, 115406 (2013).

[7] J. Pellicer-Porres, A. Segura, Ch. Ferrer-Roca, D. Martínez-García, J. A. Sans, E. Martínez, J. P. Itié, A. Polian, F. Baudelet, A. Mñnoz, P. Rodríguez-Hernández, and P. Munsch, Phys. Rev. B **69**, 024109 (2004).

[8] T. Aoyama, A. Miyake, T. Kagayama, K. Shimizu, and T. Kimura, Phys. Rev. B **87**, 094401 (2013).

[9] N. Terada, Y. Tsuchiya, H. Kitazawa, and N. Metoki, J. Korean Phys. Soc. **62**, 1905 (2013).

[10] O. Crottaz and F. Kubel, Z. Kristallogr. **211**, 482 (1996).

[11] J. Topfer, M. Trari, P. Gravereau, J. P. Chaminade, and J. P. Doumerc, Z. Kristallogr. **210**, 184 (1995).

[12] F. Damay, M. Poienar, C. Martin, A. Maignan, J. Rodriguez-Carvajal, G. André, and J. P. Doumerc, Phys. Rev. B **80**, 094410 (2009).

[13] W. M. Xu, M. P. Pasternak, and R. D. Taylor, Phys. Rev. B **69**, 052401 (2004).

[14] G. Yu. Machavariani, M. P. Pasternak, G. R. Hearne, and G. Kh. Rozenberg, Rev. Sci. Instrum. **69**, 1423 (1998).

[15] A. D. Chijioke, W. J. Nellis, A. Soldatov, and I. F. Silvera, J. Appl. Phys. **98**, 114905 (2005).

[16] A. P. Hammersley, ESRF, Internal Report No. ESRF 97HA02T, 1997 (unpublished).

[17] A. P. Hammersley, S. O. Svensson, M. Hanfland, A. N. Fitch, and D. Häusermann, High Pressure Res. **14**, 235 (1996).

[18] A. C. Larson and R. B. Von Dreele, General Structure Analysis System (GSAS), Los Alamos National Laboratory, Report No. LAUR 86-748, 1994.

[19] B. H. Toby, J. Appl. Crystallogr. **34**, 210 (2001).

[20] S. Pascarelli, O. Mathon, M. Munoz, T. Mairs, and J. Susini, J. Synchrotron Radiat. **13**, 351 (2006).

[21] A. Dadashev, M. P. Pasternak, G. Kh. Rozenberg, and R. D. Taylor, Rev. Sci. Instrum. **72**, 2633 (2001).

[22] See Supplemental Material at http://link.aps.org/supplemental/10.1103/PhysRevB.101.245121 for a detailed discussion of the lattice properties of Cu*M*O under pressure.

[23] Y. D. Kondrashev, Sov. Phys. Crystallogr. **3**, 703 (1958).

[24] F. Birch, J. Geophys. Res.-Solid Earth **91**, 4949 (1986).

[25] W. Dannhauser and P. A. Vaughan, J. Am. Chem. Soc. **77**, 896 (1955).

[26] A. B. Garg, A. K. Mishra, K. K. Pandey, and S. M. Sharma, J. Appl. Phys. **116**, 133514 (2014).

[27] In fact, one can suggest an existence of two steplike increases by ∼0.4 eV of the Cu *K*-edge energy: first at about 30 GPa, and then near 40 GPa. However, due to large error bar values it is hard to draw certain conclusions.

[28] I. G. Austin and N. F. Mott, Adv. Phys. **18**, 41 (1969).

[29] N. F. Mott, *Metal-Insulator Transitions* (Taylor & Francis Ltd., London, 1990).

[30] "Chemical shift" due to valence change is usually several eV, while the effect due to ligands and geometrical changes is smaller, typically around 1 eV or less. In the case of $CuMnO_2$ the steep change of the Cu K-edge position is ∼0.9 eV, which is consistent with all mentioned reasons.